Nanoscale Morphology of Poly(styrene-*ran*-methacrylic acid) Ionomers: The Role of Preparation Method, Thermal Treatment, and Acid Copolymer Structure

Nicholas M. Benetatos and Karen I. Winey*

Department of Materials Science and Engineering, University of Pennsylvania, Philadelphia, Pennsylvania 19104-6272

Received October 1, 2006; Revised Manuscript Received March 1, 2007

ABSTRACT: This study probes the importance of preparation method, thermal treatment, and monomer structure in determining the nanoscale morphology of ionomers using both X-ray scattering and scanning transmission electron microscopy (STEM). A Cu-neutralized poly(styrene-*ran*-methacrylic acid) (SMAA) ionomer was isolated from solution by three different methods (room temperature solvent casting, solvent casting at elevated temperature, and precipitation) having different rates of nanoscale structure formation. While both solvent cast films exhibit typical ionomer scattering and uniform spherical ionic aggregates via STEM, the precipitated material shows no ionomer scattering peak and STEM imaging detects Cu-rich regions of various size, shape, and separation. Upon annealing the precipitated material, the morphology becomes indistinguishable from that prepared by solvent casting, indicating that thermal treatment drives the metastable morphology of precipitated Cu-SMAA ionomers toward a lower energy state. Next, the influence of chain packing on the self-assembly of nanoscale ionic aggregates was probed by comparing Cu-SMAA with Cu-neutralized poly(3-methylstyrene-*ran*-methacrylic acid) (3MeSMAA). When solvent cast, the ionic aggregates are larger in Cu-3MeSMAA than Cu-SMAA, though after annealing the two ionomers are indistinguishable by X-ray scattering and STEM. Thus, while solvent casting produces near-equilibrium morphologies in Cu-SMAA, this method produces a metastable morphology in Cu-3MeSMAA. In this ionomer, near-equilibrium ionic aggregates are promoted by ensuring both slow morphological development while isolating the neutralized polymer from solution and sufficient chain mobility to maximize the local ionic interactions between the anions and cations in the ionic aggregates. More broadly, the data from Cu-3Me-SMAA constitute the first report of direct correspondence between a change in the position of the ionomer scattering peak and an increase in ionic aggregate size as observed in STEM.

Introduction

Because of their superior chemical and physical properties, ionomers find application in a variety of areas including chemically resistant thermoplastics, durable coatings, and selectively permeable ion-transport membranes.[1] The unique properties of ionomers result from the self-assembly of anionic functional groups and cations into nanoscale aggregates that act as transient physical cross-links. The morphology of ionomers has been studied using a variety of analytical techniques including small-angle X-ray scattering (SAXS), nuclear magnetic resonance (NMR), X-ray absorption spectroscopy (EXAFS), atomic force microscopy (AFM), and melt rheology, to name only a few.[2−24] Despite extensive research efforts, data are still fragmentary due to the enormous number of variables relevant in the synthesis, materials chemistry, preparation, and processing of ionomers. Establishing how the nanoscale morphology is affected by chemical, physical, and processing parameters is essential to continuing the development of this important category of polymers.

X-ray scattering has been used to detect significant morphological changes upon thermal treatment. Typical scattering patterns exhibit a single, broad, isotropic peak between 0.5 and 5 nm^{-1}. Regarding morphology changes with thermal treatment, Weiss et al. used SAXS to investigate the morphology of Zn- and Na-neutralized poly(styrene-*ran*-sulfonated styrene) (SPS) ionomers as a function of room temperature aging.[18,19] These materials were neutralized in solution, isolated by precipitation, compression-molded, heated to 300 °C, and quenched prior to SAXS experiments. Na-neutralized SPS showed an ionomer scattering peak at $q = 1.0$ nm^{-1} that shifted upward to $q = 1.7$ nm^{-1} after aging 6 months at room temperature. In contrast, Zn-neutralized SPS (prepared by identical methods) showed an ionomer peak at $q = 1.7$ nm^{-1} that remained constant upon room temperature aging. The thermally induced morphology transformation observed at room temperature in Na-neutralized SPS can only be broadly described as a change in size scale because few details about this morphology are provided by X-ray scattering alone.

X-ray scattering has also been used to explore morphology differences arising from the chemical nature of the copolymer. The scattering peak characteristic of ionomers is most often attributed to interparticle interference among a correlated array of nanostructures and interpreted using the Yarusso−Cooper model of modified hard spheres. For example, interpreting scattering data from SPS ionomers (showing an ionomer scattering peak at ∼1.7 nm^{-1}) in this manner indicates a homogeneous array of spherical ionic aggregates with average diameter of 2 nm.[22,23] In contrast, semicrystalline poly(ethylene-*ran*-methacrylic acid) (EMAA) ionomers show a broad and asymmetric ionomer peak at $q \sim 3.0$ nm^{-1} that, when interpreted by the Yarusso−Cooper model, indicates an ionic aggregate diameter of only ∼0.8 nm. The size and number density of the ionic aggregates are relatively unaffected by the choice of neutralizing counterion or the level of neutralization in both SPS and EMAA ionomers. However, there is a significant difference between ionomers based on the chemical nature of the copolymer, where SPS and EMAA differ in both the

* To whom correspondence should be addressed.

10.1021/ma062270t CCC: $37.00
Published on Web 04/03/2007

majority monomeric unit (styrene vs ethylene) and the acid type (sulfonic acid vs carboxylic acid). The relative importance of these two contributions from the copolymer structure on the ionomer morphology remains uncertain.

X-ray scattering studies typically rely on structural analysis without an independent confirmation of the assumed morphology. Scanning transmission electron microscopy (STEM), in which high-resolution imaging can be achieved with image contrast generated by differences in local average atomic number (Z), enabled the first direct visualization of the ionic aggregates in thin sections microtomed from bulk ionomers.[25,26] Furthermore, STEM has revealed the complexity of ionomer morphologies as a function of polymer backbone type, counterion type, and preparation/processing methods.[27−31] These STEM studies featured a variety of ionomers prepared from different acid copolymers (EMAA, SPS, polydimethylsiloxane) with different characteristic chain architectures. Moreover, the ionomers were neutralized and isolated by various methods including solvent casting, precipitation, and freeze-drying. In light of the vast differences between materials and preparation methodologies, the experimentally observed diversity in the size, shape, and spatial distribution of the ionic aggregates as determined from STEM imaging is not unexpected, but overall the objective of the earlier STEM investigations was not to provide insights into the origins of the various ionomer morphologies.

Recently, we have used a combination of STEM imaging and X-ray scattering to comprehensively characterize a specific ionomer: solution neutralized, solvent cast, Cu-neutralized poly(styrene-*ran*-methacrylic acid) (Cu-SMAA).[32,33] Our results provided the first report of quantitative agreement between the size and number density of the ionic aggregates determined from both real-space morphological data, measured by STEM, and reciprocal space scattering data interpreted using the Yarusso−Cooper model. This correspondence presents strong evidence that the Yarusso−Cooper scattering model accurately describes the morphology of this particular ionomer and highlights the advantage of using real-space imaging to complement and facilitate the interpretation of scattering data.

Here we systematically investigate how the nanoscale morphology of Cu-SMAA is affected by preparation methods, thermal history, and comonomer structure. We apply a combination of imaging and scattering methods and correlate the changes in the scattering pattern with changes in the nanoscale morphology observed directly using STEM. Specifically, Cu-SMAA is neutralized in solution and isolated by typical methods, namely solvent casting (at both room temperature and elevated temperature) and precipitation. These three methods allow for different rates of structure formation. After isolation, the Cu-SMAA ionomers were each subjected to thermal treatments to remove residual volatiles and allow for molecular rearrangement. Finally, we compare our results from Cu-SMAA with those of Cu-neutralized poly(3-methylstyrene-*ran*-methacrylic acid) (3MeSMAA) ionomers. The only distinction between the SMAA and 3MeSMAA copolymers is the presence of a methyl group at the meta position of the aromatic ring for each PS unit. Thus, we explore how a small perturbation in chemical structure affects the nanometer scale organization of ionic aggregates.

Experimental Section

Materials and Neutralization Procedure. Poly(styrene-*ran*-methacrylic acid) (SMAA) copolymer (7.2 mol % MAA) and poly(3-methylstyrene-*ran*-methacrylic acid) (3MeSMAA) copolymer (6.9 mol % MAA) were synthesized via bulk free radical copolymerization. Solution neutralization was performed as follows: a small quantity of copper(II) acetate monohydrate was dehydrated by heating under vacuum at ∼90−100 °C for 12 h. The appropriate stoichiometric quantity of the dehydrated copper(II) acetate salt for 100% acid neutralization was dissolved in methanol and added dropwise to a gently refluxing solution of the acid copolymer in toluene. The addition of the copper acetate solution was performed over a period of ∼30 min, and the resulting mixture was stirred for 12 h at ∼100 °C. The final solvent ratio was 90/10 toluene/methanol by volume.

Ionomer Recovery Methods. Neutralized ionomers were isolated from solution using three different methods: room temperature solvent casting (12 h, 25 °C), solvent casting at elevated temperature (0.5 h, 80 °C), and precipitation into excess methanol. For convenience, the different solvent casting preparation routes will be designated as SC25 and SC80, respectively. In each case, the resulting ionomer film or powder/precipitate was subjected to a standard thermal treatment (12 h, 80−90 °C, under vacuum) to remove volatiles and stored under anhydrous conditions. The ionomers were subsequently annealed under vacuum for 5 days at 150 °C. The unannealed and annealed materials will be designated with the suffix "Std" and "Ann", respectively. The presence of residual solvent was determined by thermogravimetric analysis (TGA) using a TA Instruments SDT 2960. Weight loss as a function of temperature data were collected by heating the sample from room temperature (25 °C) to 400 °C at a rate of 1 °C/min. TGA data indicate that materials subjected to standard thermal treatments (Std) contain ∼2 wt % residual solvent, while annealed materials (Ann) contain a negligible amount of residual solvent.

X-ray Scattering. The SAXS apparatus consists of a Nonius FR591 rotating-anode generator operated at 40 kV × 85 mA, mirror-monochromator focusing optics, an evacuated flight path, and a Bruker HiSTAR multiwire two-dimensional detector. Scattering data from ionomer films and precipitated powders (in sealed glass capillary tubes) were acquired over 1 h intervals at a sample−detector distance of 11 cm. 2D data reduction, analysis, and curve fitting were performed using Datasqueeze software.

The scattering data were modeled as previously described using the summation of three functions and a constant.[32,33] The ionomer interparticle scattering peak was fit with the Yarusso−Cooper scattering model with four independent fitting parameters: the ionic aggregate radius R_1, the radius of closest approach R_{CA} that limits the spatial correlation between two aggregates, the average sample volume per aggregate V_p, and the peak amplitude A which incorporates all of the factors affecting the absolute value of intensity. The polymerization peak and amorphous halo from the SMAA copolymer were each fit with a Lorentzian function, and an additive constant (C) was included to account for instrumental background scattering. A least-squares regression was used to determine the independent fitting parameters which yield the best fit to the scattering data.[34] The chi-squared values (a measure of how well a model fits scattering data) are less than 2, indicating good agreement between the data and our model.

Specimen Preparation and STEM. STEM specimens were microtomed from bulk solvent cast ionomer films using a Reichert-Jung ultra-microtome equipped with a diamond knife. Precipitated powders were dried under vacuum (Std) and compression-molded into films (5 h, 120 °C) prior to microtoming. All materials were sectioned at room temperature using a cutting speed of 0.2−0.4 mm/s and a nominal section thickness between 30 and 50 nm. STEM experiments were performed on a JEOL 2010F field emission electron microscope operated at 197 kV with a 70 μm condenser aperture. Images were acquired using a high angle annular dark field (HAADF) scintillating detector with linear intensity response. The collection angle was 50−115 mrad. The average diameter of the ionic aggregates was determined by individually fitting the intensity profiles across >40 ionic aggregates with Gaussian functions.[32,35] For presentation purposes, image enhancement was performed with Adobe Photoshop 5.0 using standard techniques including gray level adjustment and brightness/contrast manipulation; enhancements were applied uniformly to entire images.

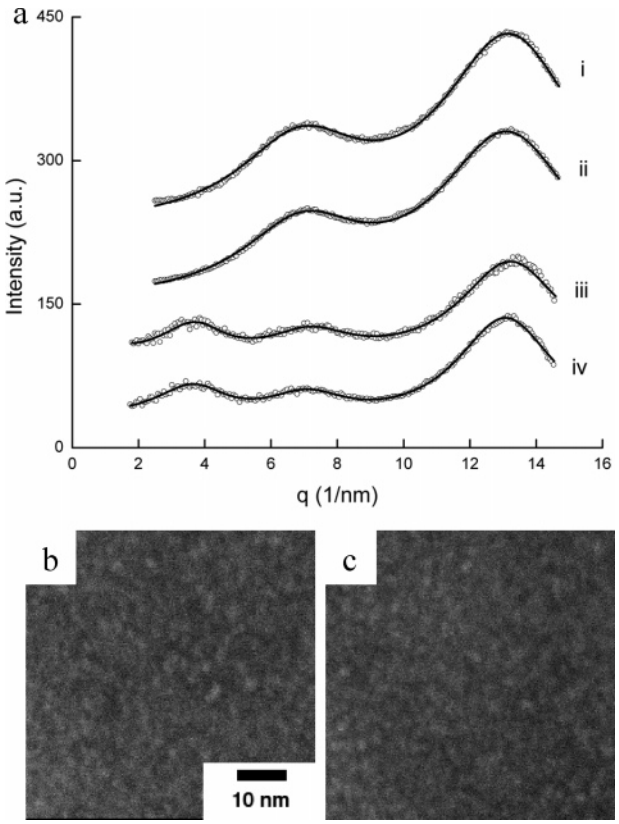

Figure 1. (a) Scattered X-ray intensity as a function of q and best fit scattering model (lines) for (i) PS homopolymer, (ii) SMAA acid copolymer, (iii) SC25 Cu-SMAA Std, and (iv) SC25 Cu-SMAA Ann ionomers. Fitting parameters are summarized in Table 1. HAADF STEM images depict a uniform, dense population of spherical ionic aggregates in both (b) SC25 Cu-SMAA Std and (c) SC25 Cu-SMAA Ann.

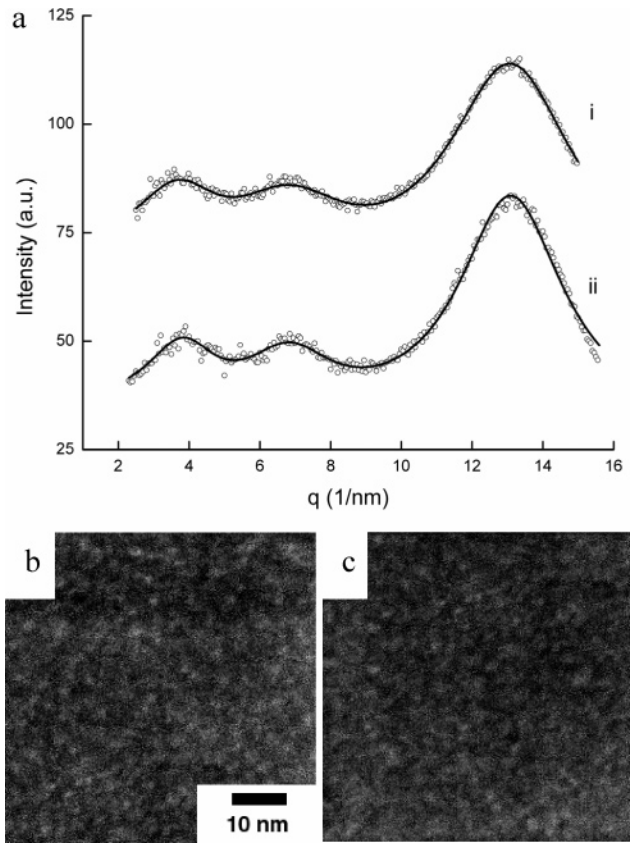

Figure 2. (a) Scattered X-ray intensity as a function of q and best fit scattering model (lines) for (i) SC80 Cu-SMAA Std and (ii) SC80 Cu-SMAA Ann ionomers. HAADF STEM images depict similar nanoscale morphologies in both (b) SC80 Cu-SMAA Std and (c) SC80 Cu-SMAA Ann.

Results and Discussion

Preparation Method and Thermal Treatment. Figure 1a illustrates the similar X-ray scattering patterns from (i) PS homopolymer and (ii) SMAA copolymer. Both patterns show two broad, isotropic peaks at ~7 and ~13 nm^{-1}, respectively. These peaks, commonly referred to as the polymerization peak ($q \sim 7$ nm^{-1}) and the amorphous halo ($q \sim 13$ nm^{-1}), are typical of amorphous polystyrene and have been described in several studies.[36−38] In addition to these two features, the neutralized Cu-SMAA ionomers (iii) SC25-Std and (iv) SC25-Ann exhibit similar isotropic ionomer scattering peaks at $q \sim 3.7$ nm^{-1}. The ionomer peak confirms successful neutralization of the acid copolymer. We interpret this scattering data with our empirical model that includes the Yarusso−Cooper interparticle ionomer scattering model for a uniform distribution of monodisperse, spherical ionic aggregates as well as functions pertaining to the experimental and sample derived background.[32,33] The ionic aggregate diameter ($2R_1$), closest approach radius (R_{CA}), and average sample volume per particle (V_p) are indistinguishable before and after annealing (Table 1).

Figure 1b,c shows the HAADF STEM images of SC25-Std and SC25-Ann. These images depict a uniform density of features and are representative of the entire specimen, indicating a homogeneous distribution of ionic aggregates. The morphology depicted by these images is consistent with the projection of a dense array of spherical ionic aggregates.[33] Multiple line scans from these images were fit with Gaussian functions to yield average diameters of 1.2 ± 0.3 nm, which is consistent with the diameters obtained from SAXS data. Although annealing SC25-Std is sufficient to eliminate the small fraction of residual solvent (<2%) that persists after standard thermal treatment, both STEM and SAXS data suggest no detectable effect on ionic aggregation.

We have also investigated the morphology of Cu-SMAA ionomers isolated by solvent casting at 80 °C. While room temperature solvent casting requires 12 h to isolate a bulk ionomer film, solvent casting at 80 °C requires only 0.5 h. Figure 2a provides the scattering patterns of SC80 Cu-SMAA ionomers subjected to (i) Std and (ii) Ann conditions. As was observed in SC25, scattering data from SC80 show no change in the size, minimum separation distance, or average sample volume per upon annealing (Table 1). The STEM images of Figure 2b,c provide direct confirmation that the size, shape, and spatial distribution of the ionic aggregates in SC80 do not change upon annealing.

Table 1. Ionic Aggregate Size As Determined from STEM and Best Fit Parameters from Our Empirical Scattering Model for Cu-SMAA Ionomers as a Function of Preparation Methods and Thermal History

	SC25 Std	SC25 Ann	SC80 Std	SC80 Ann	precipitate molded Std	precipitate molded Ann
D_{STEM} (nm)	1.2	1.2	1.2	1.2	varied	1.2
$2R_1$ (nm)	1.0	1.0	1.0	1.0		1.0
R_{CA} (nm)	0.7	0.7	0.7	0.7		0.7
V_p (nm^3)	4.2	4.0	4.9	5.1		4.3

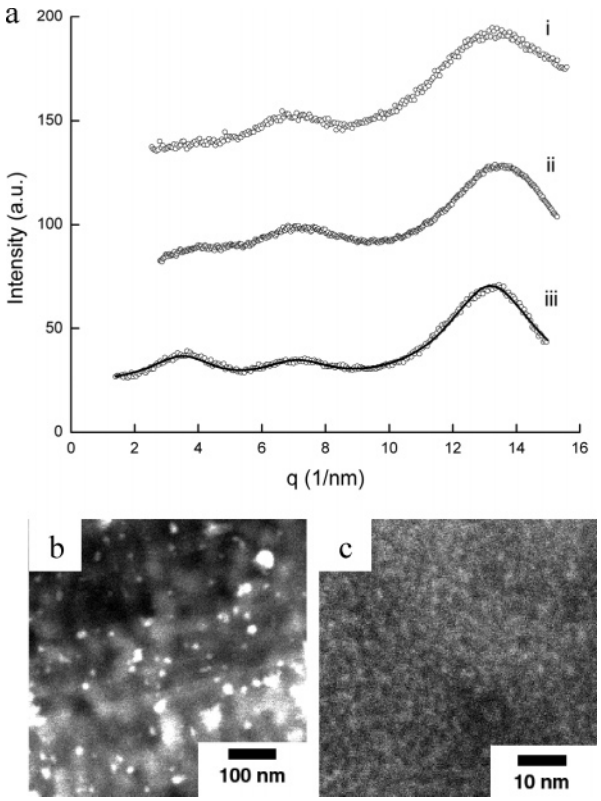

Figure 3. (a) Scattered X-ray intensity as a function of q collected from (i) precipitated Cu-SMAA Std, (ii) precipitated Cu-SMAA molded, and (iii) precipitated Cu-SMAA molded Ann. Only the annealed sample was fit with the scattering model (line). These data suggest that isolating the ionomer by precipitation induces a metastable morphology that can be driven toward equilibrium by annealing. HAADF STEM images show (b) variable sizes and separation distances of Cu-rich regions in precipitated Cu-SMAA molded and (c) a homogeneous distribution of nanoscale ionic aggregates in precipitated Cu-SMAA molded Ann.

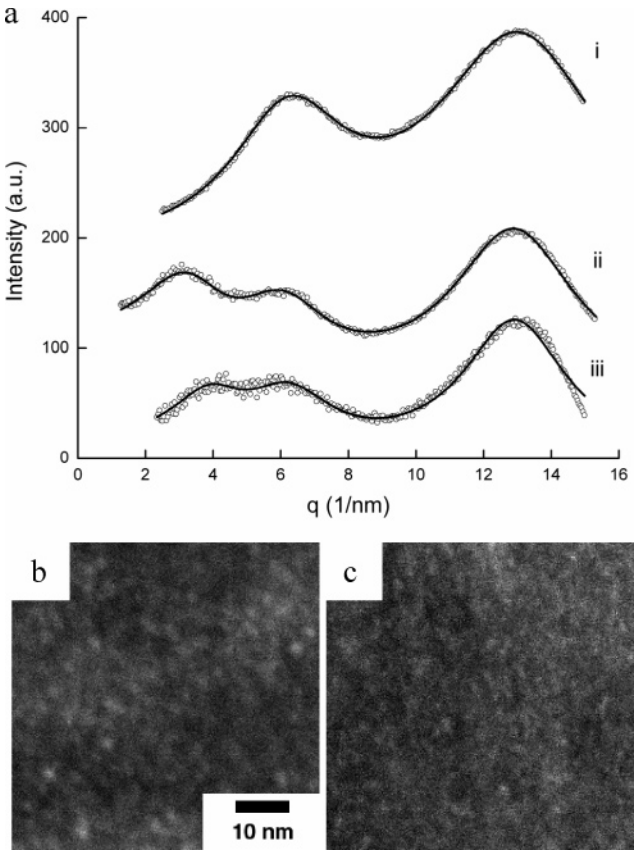

Figure 4. (a) Scattered intensity as a function of q and best fit scattering model (lines) for (i) 3MeSMAA acid copolymer, and solvent cast (SC25) ionomers (ii) Cu-3MeSMAA Std and (iii) Cu-3MeSMAA Ann. Scattering data illustrate a shift in the position of the ionomer peak after annealing. HAADF STEM images of SC25 Cu-3MeSMAA ionomers illustrate a uniform, dense population of spherical ionic aggregates in both (b) Std and (c) Ann SC 25 samples. The ionic aggregates appear slightly larger in Std (b) relative to Ann (b) materials (Table 2).

While the nanoscale morphologies of SC25 and SC80 Cu-SMAA were identical regardless of casting temperature or thermal treatments, precipitated Cu-SMAA ionomers exhibited a distinctly different morphology as characterized by STEM and X-ray scattering. Figure 3a (i) depicts the scattering pattern of precipitated Cu-SMAA Std. Contrary to the solvent cast Cu-SMAA ionomers, no ionomer peak was observed in the region between $\sim$ 2 and 5 nm^{-1}. It should be noted that this result was observed even in the case when the precipitated sample was prepared from the same solution as the solvent cast (SC25 and SC80) ionomers. The scattering pattern from precipitated Cu-SMAA Std resembles that of the unneutralized SMAA copolymer between 7 and 13 nm^{-1}; however, the scattered intensity between 2 and 5 nm^{-1} is approximately constant in precipitated Cu-SMAA Std (Figure 3a (i)), while the intensity decreases with decreasing q in the unneutralized copolymer (Figure 1a (ii)).

To further investigate this phenomenon and to facilitate STEM specimen preparation, the precipitated Cu-SMAA Std powder was compression-molded into a film (5 h, 120 °C). The scattering data did not change significantly after molding (Figure 3a (ii)). STEM images of this molded film depict a heterogeneous distribution of large (nominally 10−50 nm) Cu-rich domains (Figure 3b). These irregular, discrete objects are separated by distances ranging between 20 and 200 nm and are consistent with the absence of an interparticle scattering peak in the 2−5 nm^{-1} range. Considering that the precipitation process occurs very quickly, a nonuniform distribution of ion-rich regions should be expected. Apparently, the rapid precipitation from solution prevents the isolated acid−counterion pairs that exist in the solution of neutralized ionomer from self-assembling into nanoscale ionic aggregates and traps many of these ionic pairs in large, ion-rich domains.

After annealing the precipitated Cu-SMAA molded film, the scattering pattern exhibits an ionomer peak very similar to that obtained from the solvent cast films (Figure 3a (iii)). The best fit parameters to our empirical model (Table 1) suggest a uniform distribution of 1 nm spherical ionic aggregates after the precipitated Cu-SMAA ionomer is molded and annealed. The ionic aggregates of precipitated Cu-SMAA Molded Ann as imaged by STEM are identical to those observed in various solvent cast Cu-SMAA ionomers, i.e., spherical, with uniform spatial distribution, and comparable sizes. Evidently, the non-equilibrium morphology induced by precipitation of Cu-SMAA is metastable and can be driven toward equilibrium via thermal treatment.

Acid Copolymer Structure. In order to evaluate how the structure of the majority monomeric unit influences the development of nanoscale ionomer morphology, we compare the morphology of Cu-SMAA ionomers with Cu-neutralized 3MeSMAA ionomers prepared by identical methods (SC25) and subjected to identical thermal treatments (Std, Ann). Figure 4a (i) illustrates the scattering pattern of the unneutralized 3MeSMAA copolymer. Relative to PS and the SMAA copolymer, the polymerization peak in the scattering pattern of 3MeSMAA has shifted to lower q. Ayyagari et al. have performed molecular

dynamics simulations of atactic polystyrene that provide insight regarding the molecular origins of the polymerization peak and the amorphous halo. Their simulation results suggest that the polymerization peak arises primarily from intermolecular backbone−backbone correlations.[36] Interpreting the scattering data of Figure 4a (i) in light of these simulation results suggests that the addition of a methyl group onto the aromatic ring of each PS unit effectively increases the backbone−backbone distance in 3MeSMAA relative to that of PS and SMAA.

In addition to this shift in the position of the polymerization peak, there is a commensurate shift in the position of the ionomer peak in the scattering pattern of the solvent cast ionomer Cu-3MeSMAA Std ($q = 2.9$ nm^{-1}) relative to scattering data from solvent cast Cu-SMAA Std ($q = 3.7$ nm^{-1}) (Figure 4a (ii)). The best fit diameter of the ionic aggregates in SC25 Cu-3MeSMAA Std is $2R_1 = 1.2 \pm 0.03$ nm, a 20% increase in size compared to that previously obtained for SC25 Cu-SMAA Std ($2R_1 = 1.0 \pm 0.02$ nm). The SAXS data clearly suggest that the presence of the methyl functional group not only hinders the packing of polymer chains but also inhibits the packing of acid groups and counterions into ionic aggregates during solvent casting.

As was the case for SC25 Cu-SMAA ionomers, STEM images from SC25 Cu-3MeSMAA depict a uniform density of features that are consistent with the projection of a dense array of spherical ionic aggregates. The average ionic aggregate diameter was determined to be 1.4 ± 0.3 nm. Thus, STEM imaging supports the SAXS result that the sizes of the ionic aggregates in SC25 Cu-3MeSMAA Std are slightly increased compared to Cu-SMAA prepared and heated in the same manner (SC25, Std) (Table 2).

Figure 4a (iii) depicts the scattering pattern of SC25 Cu-3MeSMAA Ann in which the positions of the polymerization and amorphous peaks remain unchanged, while the ionomer peak has shifted to higher q (~ 3.7 nm^{-1}) relative to SC25 Cu-3MeSMAA Std. Fitting these data, we determine that the diameter of the ionic aggregates has decreased from 1.2 nm in Cu-3MeSMAA Std to 1.0 nm after annealing (Table 2). (Note that the significant overlap of the polymerization and ionomer peaks in SC 25 Cu3Me-SMAA Ann results in a large degree of uncertainty in the best fit parameters, particularly the value of V_p.) The STEM images of SC25 Cu-3MeSMAA Ann (Figure 4c) confirm the slight decrease in ionic aggregate diameter upon annealing, as the measured diameter was 1.2 ± 0.3 nm. This smaller diameter in the annealed sample is consistent with that observed in solvent cast (SC25 and SC80) Cu-SMAA both Std and Ann.

The thermal treatment does not influence chain packing in Cu-3Me-SMAA, as evidenced by no change in the positions of the polymerization and amorphous peaks after annealing. However, annealing at 150 °C (5 days) imparts enough thermal energy to the polymer chains in the immediate vicinity of the ionic aggregates that the anions and cations pack more efficiently due to electrostatic attractions, thereby reducing the diameter of the ionic aggregates in Cu-3Me-SMAA. By comparing the ionic aggregates in Cu-SMAA and Cu-3Me-SMAA, we observe that the influence of chain packing in the matrix is only evident in the metastable (Std) morphologies. In the near-equilibrium morphologies developed by annealing, the self-assembled morphology of the ionic aggregates appears to be dominated by the electrostatic interactions between the anions (COO^-) and cations (Cu^{2+}).

Table 2. Scattering Peak Positions, Average Ionic Aggregate Diameters Measured from STEM Images, and Best Fit Parameters from Our Empirical Scattering Model for Cu-3MeSMAA Ionomers

	SC25 Std	SC25 Ann
ionomer peak (nm^{-1})	2.9	3.6
polymerization peak (nm^{-1})	5.9	6.1
D_{STEM} (nm)	1.4	1.2
$2R_1$ (nm)	1.2	1.0
R_{CA} (nm)	0.8	0.7
V_p (nm^3)	9.3	3.9

With regard to preparation methods, it is important to note that room temperature solvent casting Cu-SMAA and Cu-3MeSMAA ionomers produce a near-equilibrium and a metastable morphology, respectively. Thus, depending on the chemical system, a particular preparation method may or may not produce a near-equilibrium morphology. In these ionomers a thermal treatment at 150C for 5 days was sufficient to transform even the highly nonequilibrium morphology produced by precipitation to a near-equilibrium nanoscale morphology.

More broadly, the data from Cu-3Me-SMAA constitute the first report of direct correspondence between a change in the position of the ionomer scattering peak and an increase in ionic aggregate size as observed in STEM. This agreement provides further support to our recent evidence that the Yarusso−Cooper scattering model can provide an excellent description of the nanoscale morphology of certain ionomers.

Conclusion

We have used X-ray scattering *and* STEM to study the influence of preparation method, thermal treatment, and comonomer structure in determining the morphology of ionomers. Specifically, Cu-SMAA ionomers recovered by solvent casting exhibit spherical, nanometer sized ionic aggregates, while Cu-SMAA ionomers recovered by precipitation show no interparticle scattering peak and exhibit larger, irregular ion-rich domains in STEM. Furthermore, annealing the solvent cast Cu-SMAA above the matrix glass transition temperature had no influence on the morphology, while annealing the precipitated Cu-SMAA transformed the morphology into a homogeneous assembly of nanometer-sized ionic aggregates. These data suggest that rapid precipitation of Cu-SMAA ionomers, and likely ionomers in general, induces a metastable morphology that requires a thermal treatment to achieve a lower energy state.

These results clearly demonstrate that preparation methods can significantly alter the nanoscale morphology of solution neutralized Cu-SMAA ionomers. It is expected that other ionomers, including those with a different polymer backbone or acid type, prepared by different neutralization methods, or involving other counterions, may require different preparation routes to yield equilibrium morphologies. For example, we observe that the addition of a methyl group to the styrene monomeric unit (3MeSMAA) decreases chain packing and hinders ionic aggregation during solvent casting, as evidenced by a shift toward lower q in the positions of the polymerization and ionomer scattering peaks. In this material (SC25 Cu-3MeSMAA Std), imaging and scattering data suggest a 20% increase in the diameter of the ionic aggregates relative to SC25 Cu-SMAA Std. After annealing, the ionomer scattering peak shifts to higher q, while the polymerization peak position remains unchanged. Evidently, annealing drives this metastable state toward a near-equilibrium morphology that is dominated by ionic interaction rather than matrix chain packing.

In conclusion, determining definitive structure−property relationships requires careful attention to the manner in which materials are prepared and annealed. As a consequence, caution must be exercised when comparing ionomer studies in the literature. It is imperative that future research continues to

systematically explore how the numerous processing methods and thermal treatments of ionomers affect the structure and properties, noting that these influences will differ with ionomer chemistry. Quantifying these relationships will provide an important step toward the rational design, synthesis, and preparation of superior ionomeric materials.

Acknowledgment. Funding was provided by the National Science Foundation (DMR02-35106 and DMR05-20020). The authors acknowledge Prof. Joon-Seop Kim of Chosun University for providing SMAA and 3MeSMAA copolymers. Nicholas M. Benetatos acknowledges funding provided through an Augustus T. Ashton fellowship at the University of Pennsylvania.

References and Notes

(1) Eisenberg, A.; Kim, J.-S. *Introduction to Ionomers*; John Wiley & Sons: New York, 1998; p 352.
(2) Ding, Y. S.; Hubbard, S. R.; Hodgson, K. O.; Register, R. A.; Cooper, S. L. *Macromolecules* **1988**, *21*, 1698−1703.
(3) Ding, Y. S.; Register, R. A.; Nagarajan, M. R.; Pan, H. K.; Cooper, S. L. *J. Polym. Sci., Part B: Polym. Phys.* **1988**, *26*, 289−300.
(4) Eisenberg, A.; Navratil, M. *Macromolecules* **1973**, *6*, 604−612.
(5) Grady, B. P.; Cooper, S. L. *Macromolecules* **1994**, *27*, 6627−6634.
(6) Grady, B. P.; Cooper, S. L. *Macromolecules* **1994**, *27*, 6635−6641.
(7) Hara, M.; Jar, P.; Sauer, J. A. *Polymer* **1991**, *32*, 1380−1383.
(8) Kutsumizu, S.; Goto, M.; Yano, S. *Macromolecules* **2004**, *37*, 4821−4829.
(9) Kutsumizu, S.; Hara, H.; Schlick, S. *Macromolecules* **1997**, *30*, 2320−2328.
(10) McLean, R. S.; Doyle, M.; Sauer, B. B. *Macromolecules* **2000**, *33*, 6541−6550.
(11) O'Connell, E. M.; Peiffer, D. G.; Root, T. W.; Cooper, S. L. *Macromolecules* **1996**, *29*, 2124−2130.
(12) O'Connell, E. M.; Root, T. W.; Cooper, S. L. *Macromolecules* **1994**, *27*, 5803−5810.
(13) O'Connell, E. M.; Root, T. W.; Cooper, S. L. *Macromolecules* **1995**, *28*, 3995−3999.
(14) O'Connell, E. M.; Root, T. W.; Cooper, S. L. *Macromolecules* **1995**, *28*, 4000−4006.
(15) Register, R. A.; Cooper, S. L. *Macromolecules* **1990**, *23*, 310−317.
(16) Register, R. A.; Sen, A.; Weiss, R. A.; Cooper, S. L. *Macromolecules* **1989**, *22*, 2224−2229.
(17) Weiss, R. A. *J. Polym. Sci., Polym. Phys. Ed.* **1982**, *20*, 65−72.
(18) Weiss, R. A.; Lefelar, J. A. *Polymer* **1986**, *27*, 3−7.
(19) Weiss, R. A.; Lefelar, J. A.; Toriumi, H. *J. Polym. Sci., Polym. Lett. Ed.* **1983**, *21*, 661−667.
(20) Wu, D. Q.; Chu, B.; Lundberg, R. D.; MacKnight, W. J. *Macromolecules* **1993**, *26*, 1000−1007.
(21) Wu, D. Q.; Phillips, J. C.; Lundberg, R. D.; MacKnight, W. J.; Chu, B. *Macromolecules* **1989**, *22*, 992−995.
(22) Yarusso, D.; Cooper, S. L. *Macromolecules* **1983**, *16*, 1871−1880.
(23) Yarusso, D.; Cooper, S. L. *Polymer* **1985**, *26*, 371−378.
(24) Yarusso, D.; Ding, Y. S.; Pan, H. K.; Cooper, S. L. *J. Polym. Sci., Polym. Phys. Ed.* **1984**, *22*, 2073−2093.
(25) Laurer, J. H.; Winey, K. I. *Macromolecules* **1998**, *31*, 9106−9108.
(26) Winey, K. I.; Laurer, J. H.; Kirkmeyer, B. P. *Macromolecules* **2000**, *33*, 507−513.
(27) Batra, A.; Cohen, C.; Kim, H.; Winey, K. I.; Ando, N.; Gruner, S. M. *Macromolecules* **2006**, *39*, 1630−1638.
(28) Benetatos, N. M.; Winey, K. I. *J. Polym. Sci., Part B: Polym. Phys.* **2005**, *43*, 3549−3554.
(29) Kirkmeyer, B. P.; Taubert, A.; Kim, J.-S.; Winey, K. I. *Macromolecules* **2002**, *35*, 2648−2653.
(30) Kirkmeyer, B. P.; Weiss, R. A.; Winey, K. I. *J. Polym. Sci., Part B: Polym. Phys.* **2001**, *39*, 477−483.
(31) Taubert, A.; Winey, K. I. *Macromolecules* **2002**, *35*, 7419−7426.
(32) Benetatos, N. M.; Heiney, P. A.; Winey, K. I. *Macromolecules* **2006**, *39*, 5174−5176.
(33) Benetatos, N. M.; Chan, C. D.; Winey, K. I. *Macromolecules* **2007**, *40*, 1081−1088.
(34) Heiney, P. A. *Comm. Powder Diffraction Newsletter* **2005**, *32*, 9−11.
(35) Benetatos, N. M.; Smith, B. W.; Heiney, P. A.; Winey, K. I. *Macromolecules* **2005**, *38*, 9251−9257.
(36) Ayyagari, C.; Bedrov, D.; Smith, G. D. *Macromolecules* **2000**, *33*, 6194−6199.
(37) Mitchell, G. R.; Windle, A. H. *Polymer* **1984**, *25*, 906−920.
(38) Wecker, S. M.; Davidson, T.; Cohen, J. B. *J. Mater. Sci.* **1972**, *7*, 1249−1259.

MA062270T